PROCEEDINGS OF SCIENCE

Improved RPC (iRPC) detector for CMS data taking in HL-LHC

Salvatore Buontempo[a,b]

[a] *INFN Sezione di Napoli, Napolie, Italy*

[b] *CERN Geneva, Switzerland*

In view of the challenging data taking of CMS in HL-LHC Collisions, an extensive upgrade is underway for the CMS Muon System to ensure its optimal performance in muon triggering and reconstruction. The key role of RPC as dedicated muon detectors will provide relevant timing information, profiting of their time resolution, to secure sub-bunch crossing event timestamp. To meet the requirements of LHC Phase-2, the RPC system will be expanded up to 2.4 in pseudo-rapidity. The forward Muon system's upcoming RE3/1 and RE4/1 stations will feature improved RPC (iRPC). Distinguished by a unique design and geometry, including a 2D strip readout, these iRPC represent a significant advancement over the current RPC system. The enhancements include the use of thinner electrodes, a narrower 1.4 mm gas gap, and improved FEB allowing a 30 fC threshold. At the end of 2023, two iRPC chambers were installed in the CMS detector. Present paper provides a full summary of the iRPC project.

Internacional Conference of High Energy Physics - ICHEP 2024
Prague - Czechia
July 2024

PoS(ICHEP2024)888

1. Introduction

The Muon System of the Compact Muon Solenoid (CMS) [1] is composed of four types of gaseous detectors: Drift Tubes (DT) in the barrel, Cathode Strips Chambers (CSC) and Gas Electron Multipliers (GEM) in the endcaps, and Resistive Plate Chambers (RPC) in both regions, covering up to $|\eta| = 2.4$ in pseudorapidity [2]. The existing RPC system comprises 1,056 chambers with double 2 mm gas gap each, performing with high efficiency since the beginning of CMS operation . In view of the Phase-II upgrade of the LHC, the iRPC will be installed in the challenging forward region of CMS, stations RE3/1 and RE4/1, as shown in Fig. 1a. These iRPC also feature double-gap designs, but with a narrower 1.4 mm gas gap and High-Pressure Laminated (HPL) electrodes measuring 1.4 mm in thickness. They are coupled with a new Front-End Boards (FEB) enabling a charge threshold down to 30 fC (as compared to the 150 fC threshold of the preexisting RPC detectors). The electronics is designed to be capable to operate in a region where the gamma background expected is around 700 Hz/cm^2 [3]. The new iRPC boast timing resolution superior to their predecessors, reaching around 500 ps, while the existing system can achieve 1.6 ns [4]. While the existing RPC system has a 1D readout, the narrower strip pitch and the readout on both strip ends for iRPC enhance granularity in the ϕ and η direction up to 0.3-0.6 cm and 1.5 cm, respectively [5].

The chamber components are produced at various locations worldwide, with a stringent Quality Control (QC) process ensuring that only qualified components are used to assemble chambers. Subsequent QC steps ensure that the assembled chambers are fit for installation in CMS. The mass production of iRPC chambers is ongoing at CERN and Ghent University assembly sites. The following sections present the assembly procedure and QC process of the iRPC, along with an overview of their performance metrics, including efficiency, noise level, and space and timing resolution. Performance under gamma irradiation background, chamber mass production and installation schedule in CMS detector are also presented.

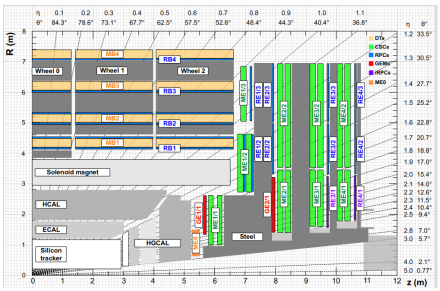

(a) Muon System of the CMS for the HL-LHC.

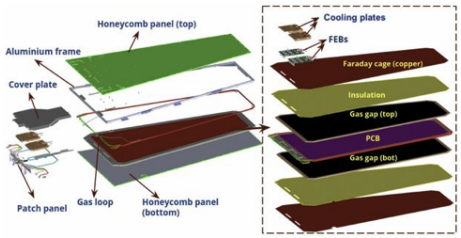

(b) Schematic view of an iRPC detector [6].

Figure 1: Muon system and iRPC layout in the CMS detector.

2. The improved Resistive Plate Chambers

The iRPC has a trapezoidal shape, similar to the existing endcap RPC chambers in CMS. Each iRPC features two 1.4 mm gas gaps formed by two 1.4 mm HPL electrodes coated with a thin graphite resistive layer of around 0.9 - 3 $\times$ 10^{10} Ω cm. Like the existing RPC, the strips for signal

readout are placed between the two gaps, but in iRPC they are integrated into a large trapezoidal printed circuit board (PCB), which is divided into left and right sections, each containing 48 readout strips. The strip pitch is approximately 12.3 mm at the high radius (HR) and 6 mm at the low radius (LR). Innovative strip PCB design allows the transfer of LR side signal for each strip to the HR region with a return line, printed in PCB. In that way, the FEB can collect both LR and HR side signals being located on top of the high radius (lowest radiation dose region of the chamber) and to group all services (HV and LV cabling, gas and cooling piping) only in that region. The schematic view of an iRPC chamber is presented in Fig. 1b.

A new electronics system featuring low-noise FEB has been designed and developed. These FEBs are fast, reliable, and can withstand high radiation environments [7]. They transmit digital signals to the Back-End Boards (BEBs) using the radiation-tolerant Giga-Bit Transceiver Chip (GBTx), which enables high-speed bidirectional optical links. The BEBs handle fast/slow control, data decompression, cluster finding, and angle conversion, and they send trigger primitives to the End Cap Muon Track Finder (EMTF) and the Data Acquisition (DAQ) system [8].

3. Chamber Assembly and Quality Control

The QC process is divided into four distinct steps. The first two are conducted at the component level prior to chamber assembly, while the latter two take place after the assembly. The initial QC process is performed at the original manufacturing sites. For instance, the KODEL Laboratory in South Korea uses the HPL pieces produced in Italy to manufacture the gas gaps, which undergo QC tests before being shipped to the iRPC assembly sites in Ghent and CERN. Upon arrival at the assembly sites, all QC procedures are repeated to ensure no damage occurred during transportation.

The QC process for gas gaps involves four distinct tests. The process begins with a visual inspection to identify any scratches or broken inlets that would render the gap unsuitable for chamber assembly. Following the visual inspection, the gap is filled with Argon gas to a over pressure of up to 16 mbar and then sealed. The pressure drop is monitored over a 10-minute period to detect leaks; a pressure drop of less than 0.4 mbar qualifies the gap for the subsequent test.

Next, the spacer bonding test is conducted. Gas gaps contain spacers that maintain a constant separation of 1.4 mm across the entire gap surface. External pressure is applied to the spacer regions to ensure proper bonding, with smooth pressure transitions across all spacers expected, as in Fig.

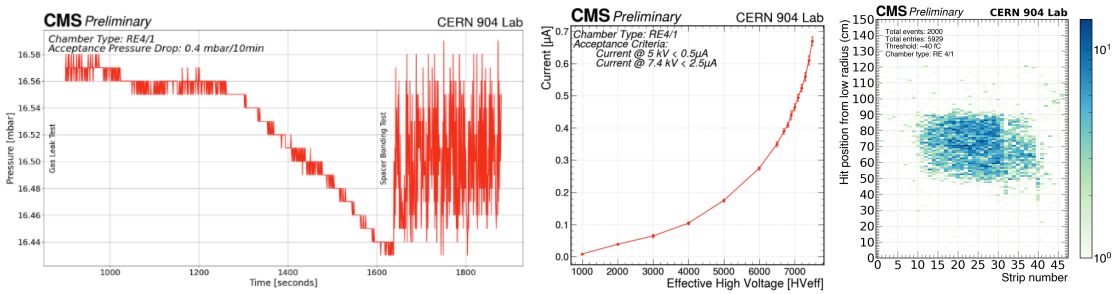

(a) Gap leak test and spacer bonding pressure test. **(b)** The current test for gaps. **(c)** The 2D hits position at WP.

Figure 2: QC results of gaps and chamber.

2a. Any irregularities, such as spikes in the pressure curve, may indicate a popped spacer, which would disqualify the gap from proceeding to the next QC step.

The final QC test for the gas gap is a high voltage scan, designed to verify the proper functioning of both the connector and the gas gap under high voltage conditions. During the scan, the gas gap is filled with the standard RPC gas mixture used in CMS, composed of 95.2% of $C_2H_2F_4$, 4.5 % of iC_4H_{10} and 0.3 % of SF_6. The behavior of the gas gap is monitored under increasing voltage to verify its functionality. Below 6250 V, the response should be due to ohmic properties, while above this voltage, an exponential increase in current is expected due to secondary ionization from ionized particles in the gas, as illustrated in Fig. 2b. The current must not exceed 0.5 μA at 5000 V, known as the standby voltage, and must remain below 2.5 μA at 7400 V, approximately the operating voltage.

Once all components pass QC validation, they can be used for chamber assembly, after which the QC process continues at the chamber level. Initially, a leak test as the one provided at the gap level is performed to ensure that the gas piping and connections are properly sealed. The next step involves a test with cosmic rays, utilizing three scintillators for cosmic muon coincidence and one scintillator for vetoing cosmic showers. Since each chamber is equipped with two FEBs and two strip PCBs (left and right), each chamber undergoes the cosmic QC process twice — once for the left side and once for the right side. Fig. 2c depicts the hit position profile in the 30 x 40 cm^2 coincidence region with the chamber in the working point (WP = 7060 V). The hit position from LR is calculated using the arrival time difference between both strip ends ($t_2 - t_1$), according to the following equation $r = \frac{1}{2}L - \frac{(t_2-t_1)}{2}v$, where L is the length of the readout strip and v is the signal speed.

The resolution along the x-axis (corresponding to ϕ in CMS coordinate system) is determined by the strip pitch (from 6 mm to 12.3 mm). In contrast, the resolution along the y-axis (η) is constrained by the intrinsic timing resolution of the FEB TDC channels (≈150 ps), resulting in a spatial resolution in η region of approximately 1.6 cm [9].

As part of the test with cosmic rays, four scans are performed in total: three efficiency scans with different chamber configurations (double gap, top gap and bottom gap) and a noise scan using a dedicated random trigger. Fig. 3a presents an efficiency plot for a double gap scan with a cosmic trigger, where the efficiency at each point is defined as the ratio of detected muons to the total number of triggers. A detected muon is considered to have at least one hit within the scintillator's projected area. With varying the time Readout Window (RxLW), the maximum efficiency, efficiency at the working point and working point itself remain consistent at 99%, 98%, and 7060 V, respectively. The working point is defined as the minimum high voltage value giving an efficiency of at least 95% plus 150 V.

The muon cluster size at the working point, shown in Fig. 3b, is defined as the number of consecutive strips fired when a muon crosses the RPC detector. With a strip pitch in the scintillator coincidence region of approximately 1 cm, the mean cluster size is around 2.6 cm. This is within the requirements, as a high cluster size can negatively impact spatial resolution. Fig. 3c shows the noise rate at the working point. The noise rate is measured by counting the number of hits within a variable time window. The ratio of hits to readout time provides the observed noise, which is then divided by the active detector area (strip area) to obtain the rate per square centimeter. The mean noise rate should be lower than 5 Hz/cm^2.

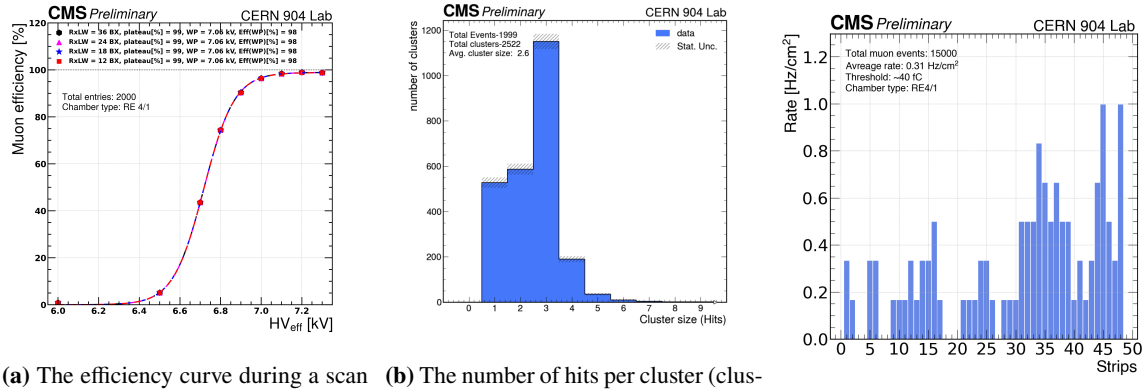

(a) The efficiency curve during a scan with cosmic muons.

(b) The number of hits per cluster (cluster size) distribution.

(c) The noise distribution at the WP.

Figure 3: Efficiency and noise scan for iRPC chamber QC.

The next step in the QC process is a long term stability test, where the iRPC chambers are powered up to and kept at the working point for one month to verify that the currents remain stable over an extended period. For a chamber to be considered qualified, the current must remain stable below 2.5 μA. The chamber is not accepted when the current increase is higher than 50% and not related with environmental parameters (pressure, temperature and humidity). Before installation in CMS, a final QC step will be conducted with CMS like conditions, at CERN assembly laboratory, with the final FEB electronics attached to the chamber.

4. Performance of iRPC under gamma background

To validate the performance of an iRPC chamber with high background conditions similar to those expected in CMS during HL-LHC (2 kHz/cm^2, including a factor x3 safety margin), during last June 2024 we performed a test beam measurement at Gamma Irradiation Facility (GIF++)) at CERN, using a muon beam around 150 Gev/c. In parallel the chamber was irradiated with 12 TBq ^{137}Cs gamma source of 662 keV, providing a tunable background condition using different absorption factors. In Fig. 4b, we show the event display in the chamber without any background. The muon beam spot can be reconstructed thanks to the strips readout in both ends. The plot shows the muon reconstruction without offline realignment.

In Fig. 4c, we show the efficiency curves detected with different background conditions (from zero up to 2.3 kHz/cm^2) demonstrating the capability to secure up to 96% efficiency even with 1 kHz/cm^2 background. Efficiency curves were recorded with energy threshold of 40fC and a trigger window of 12 BX (below the one requested to operate in CMS during HL-LHC). The working point increases with background gamma rate due to the ohmic contribution in the current, but iRPC chamber WP was never exceeding 7.3 kV, even up to 2.3 kHz/cm^2.

5. iRPC chamber mass production and installation in CMS

Pilot production of prototype iRPC chambers was started in 2021. 4 demonstrator chambers (2 type 3.1 and 2 type 4.1) were installed in CMS detector in positions RE+4/1/15,16 and RE+3/1/15,16 during last months of the Long Shutdown 2 (2021-22), using preliminary version of FEBs. Main

goal was to validate in real working environment: Noise < 1Hz/cm^2 using final end cap disk grounding, FEB temperature stable in CMS endcap closed mode with water cooling, HV currents showing smooth operation during LHC Run III and normal operation in 3.8 T magnetic field.

In Fig. 5b average noise of about 0.2 Hz/cm^2 is shown in one of 2 chambers installed in RE+3.1. Mass production of iRPC chamber has started in summer 2023 and is expected to end by fall 2024. As shown in Fig. 5a, during last Year-End Technical Stop (YETS) in December 2023, we installed in CMS RE-3/1/16 and RE-3/1/18 positions 2 final chambers produced at beginning of iRPC mass production, equipped with first example of FEBs final version.

All iRPC services are already installed since LS2 in CMS waiting for all 72 chambers to be installed in next YETS planned before LHC Long Shutdown 3 (LS3).

6. Conclusion

The iRPC designed for the CMS Muon System mark a notable leap forward in detector technology. Featuring narrower gas gaps and improved timing resolution, these chambers are tailored for the challenging conditions of the LHC Phase-II upgrade. Rigorous QC procedures, spanning from component-level checks to final chamber performance assessments under CMS-like conditions, ensure their reliability and operational readiness. This advancement not only enhances muon detection accuracy but also underscores their pivotal role in advancing particle physics research at the forefront of experimental science. The mass production and QC of the iRPC are progressing smoothly at both CERN and Ghent University assembly sites. Four demonstrators chambers installed during the Long Shutdown 2 (2021) have shown normal operation with low noise (< 1Hz/cm^2) and stable temperature [10]. Studies conducted at GIF++ demonstrated high performance under a high gamma background rate, within a safety factor of 3 compared to what is expected at CMS [11]. The first 2 mass production chambers were installed in the CMS cavern in the YETS 2023/2024, with the remaining 70 chambers scheduled for installation during YETS before LS3.

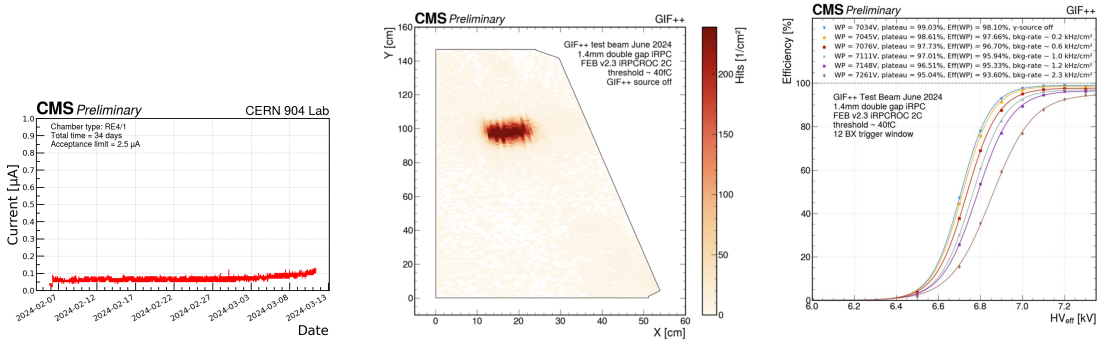

(a) Long term (1 month) monitored current.

(b) Event display with muon beam at GIF++.

(c) Efficiency curves for different background gamma rates.

Figure 4: Long term stability and iRPC results from GIF++.

Acknowledgments

We would like to acknowledge the enduring support for the Upgrade of the CMS detector and the supporting computing infrastructure provided by the following funding agencies: FWO (Belgium); CNPq, CAPES and FAPERJ (Brazil); MES and BNSF (Bulgaria); CERN; CAS, MoST, and NSFC (China); MINCIENCIAS (Colombia); CEA and CNRS/IN2P3 (France); SRNSFG (Georgia); DAE and DST (India); IPM (Iran); INFN (Italy); MSIP and NRF (Republic of Korea); BUAP, CINVESTAV, CONACYT, LNS, SEP, and UASLP-FAI (Mexico); PAEC (Pakistan); DOE and NSF (USA).

References

[1] M. A. Shah, et al., JINST 14 (2019) C11012. doi:10.1088/1748-0221/14/11/C11012.

[2] CMS Collaboration, JINST 3 (2008) S08004. doi:10.1088/1748-0221/3/08/S08004.

[3] P. Kumari, et al (2020). arXiv:2005.11396.

[4] J. Song, et al. (7 2024). doi:10.1007/s41605-024-00473.

[5] K. Shchablo, et al., JINST 16 (2021) C05002. doi:10.1088/1748-0221/16/05/C05002.

[6] A. Samalan, et al., JINST 17 (2022) C01011. doi:10.1088/1748-0221/17/01/C01011.

[7] M. Gouzevitch, et al., NIM A 1064 (2024) 169400. doi:10.1016/j.nima.2024.169400.

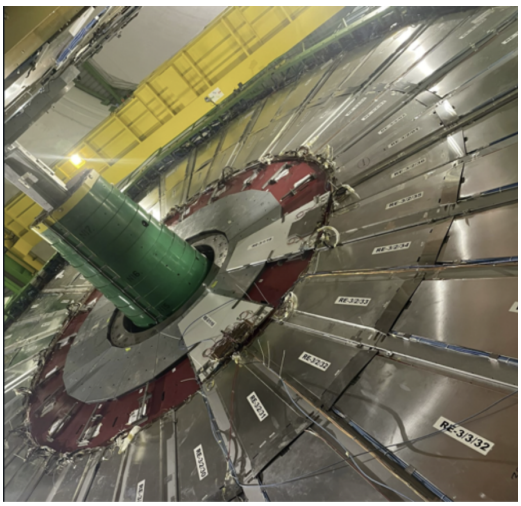

(a) First two final iRPC chambers RE-3/1/16 and RE-3/1/18 installed in the negative endcap of CMS detector in December 2023. The iRPC chambers are expected to be included in CMS muon reconstruction by Run 4.

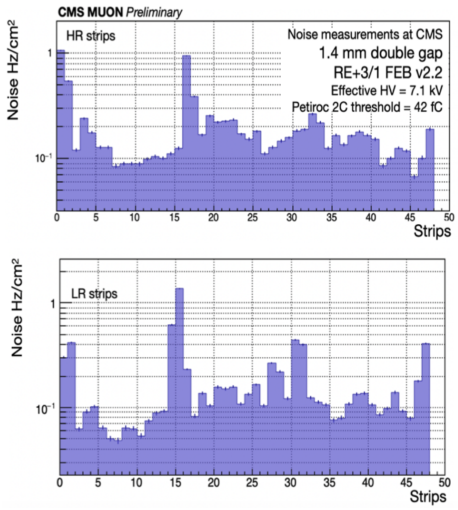

(b) Average noise per strip end in the low radius and high radius sides, recorded in one of two iRPC demonstrator chambers RE+3/1 installed in CMS detector during YETS in January 2022.

Figure 5: iRPC chambers installed in P5 and noise results.

[8] H. Kou, et al., Rad. Det. Tech. Meth. 6 (2022) 306–316. doi:10.1007/s41605-022-00340-6.

[9] M. Gouzevitch, et al., NIM A 1064 (2024) 169400. doi:10.1016/j.nima.2024.169400.

[10] E. Asilar, et al., NIM A 1048 (2023) 167953. doi:10.1016/j.nima.2022.167953.

[11] A. Samalan, et al., NIM A 1060 (2024) 169075. doi:10.1016/j.nima.2024.169075.